This article has been accepted for inclusion in a future issue of this journal. Content is final as presented, with the exception of pagination.

A Relativistic and Electromagnetic Correction to the Ramo–Shockley Theorem

Dion Li, *Student Member, IEEE*, David Chernin, and Y. Y. Lau, *Fellow, IEEE*

***Abstract*— The classical Ramo–Shockley (RS) theorem gives the current induced on perfect conductors by the motion of nearby charges, assuming nonrelativistic motion of those charges in electrostatic fields. This article illustrates how relativistic and electromagnetic effects modify RS in some simple examples. Specifically, we present explicit, closed form analytic solutions of Maxwell's equations for the induced current distribution on perfectly conducting plates due to the motion of a line charge moving parallel and perpendicular to the plates. The results have been verified by several methods, including particle-in-cell simulations. They are compared with the classical electrostatic theory used to derive RS. New insights into the limitation and validity of RS are provided. Electromagnetic shocks are explicitly calculated in closed form when the line charge strikes a parallel plate transmission line.**

***Index Terms*— Induced current, Ramo's theorem, Ramo–Shockley (RS) theorem, Shockley–Ramo theorem.**

I. Introduction

As a charge moves in a vacuum among grounded conductors, currents are induced on the conductors due to the rearrangement of the surface charge. An elegant expression for the induced current is given by Ramo [1] and Shockley [2], known as Ramo's theorem or the Ramo–Shockley (RS) theorem. The basic idea is that as a charge moves from one place to another, the surface charge on surrounding conductors change, resulting in an induced current on these conductors. This induced current can be measured (for radiation detection [3]), or can be used to drive a load (for radiation generation using an electron beam [4]). Additional applications include accelerator theory [5], [6], discharge physics [7], semiconductor devices [8], [9], and protein dynamics [10]. RS is thus a very powerful theorem with broad utility.

RS assumes that the charge motion is nonrelativistic so that at any instant of time, the electric field distribution is given by the instantaneous electrostatic field due to the space charge, thereby ignoring relativistic and electromagnetic effects. This deficiency has rarely been addressed in the literature, as far as we have been able to determine. In this article, we display these effects with explicit, simple closed form solutions, for the first time. Our model consists of a line charge moving parallel and perpendicular to an infinitely conducting plate [Fig. 1(a)], and perpendicular to two parallel, infinitely conducting plates [Fig. 1(b)]. In both geometries, we derived the induced current on the conductor that is relativistically and electromagnetically correct. Different methods were used to obtain these solutions numerically. In all cases studied in this article, we were able to obtain closed form, analytic solutions. They are compared with the corresponding solutions under the electrostatic approximations. Our closed form solutions explicitly illustrate the generation of an electromagnetic shock wave when the line charge strikes a conducting plate and is removed from the region, a phenomenon completely absent in the electrostatic approximation of RS.

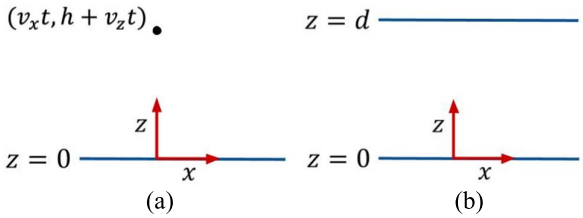

Fig. 1. Line charge initially located at $(x, z) = (0, h)$ in (a) single-plate geometry and (b) parallel-plate geometry.

In Section II, we consider the single plate geometry [Fig. 1(a)] in which the line charge either moves parallel or perpendicular to the conducting plate. In Section III, the line charge is assumed to move perpendicular to two conducting plates [Fig. 1(b)], as in a simple diode. The induced current on the lower conducting plate is computed by several methods, including a 2-D particle-in-cell simulation, all showing excellent agreement. The derivations of the analytic solutions are given in the Appendices. Concluding remarks are given in Section IV.

II. Single Plate

Let λ be the line charge density of an infinitely long rod of infinitesimal cross section. The rod is initially located at $(x, z) = (0, h)$ above a single perfectly conducting plate at $z = 0$ [Fig. 1(a)]. In a quasi-static description, this line charge

Manuscript received May 26, 2021; accepted July 19, 2021. This work was supported in part by the Air Force Office of Scientific Research (AFOSR) under Grant FA9550-18-1-0153 and Grant FA9550-18-1-0062, and in part by the L3Harris Electron Devices Division. The review of this article was arranged by Senior Editor F. Taccogna. *(Corresponding author: Y. Y. Lau.)*

Dion Li and Y. Y. Lau are with the Department of Nuclear Engineering and Radiological Sciences, University of Michigan, Ann Arbor, MI 48109 USA (e-mail: yylau@umich.edu).

David Chernin is with Leidos, Inc., Reston, VA 20190 USA.

Color versions of one or more figures in this article are available at https://doi.org/10.1109/TPS.2021.3099512.

Digital Object Identifier 10.1109/TPS.2021.3099512

This work is licensed under a Creative Commons Attribution 4.0 License. For more information, see https://creativecommons.org/licenses/by/4.0/

This article has been accepted for inclusion in a future issue of this journal. Content is final as presented, with the exception of pagination.

produces a surface charge of density σ on the plate

$$\sigma(x;t) = -\frac{\lambda z_c}{\pi[(x-x_c)^2+z_c^2]} \tag{1}$$

where (x_c, z_c) are the (x, z) instantaneous coordinates of the line charge. When there is a parallel, uniform motion of the line charge, $x_c = x_c(t) = v_x t$, $z_c = h$, a surface current, $\mathbf{K} = \mathbf{x}K_x$, on the conducting plate is induced, which is governed by the continuity equation

$$\frac{\partial \sigma}{\partial t} = -\nabla \cdot \mathbf{K} = -\frac{\partial K_x}{\partial x}. \tag{2}$$

We may write the left-hand side (LHS) of (2) as

$$\frac{\partial \sigma}{\partial t} = \frac{\partial \sigma}{\partial x_c}\frac{dx_c(t)}{dt} = v_x \frac{\partial \sigma}{\partial x_c} = -v_x \frac{\partial \sigma}{\partial x} \tag{3}$$

where we have used (1). Equating (2) and (3), we obtain the quasi-static induced current

$$K_x = v_x \sigma = -\frac{\lambda h v_x}{\pi[(x-v_x t)^2+h^2]}. \tag{4}$$

To include relativistic effects, we assume that the line charge has been moving at a constant velocity, $\mathbf{x}v_x$, from $t = -\infty$, and compute the surface current by Lorentz transformation from the frame moving with the line charge, where we may compute the electric field using the image charge method, back to the lab frame. The result is (see Appendix A)

$$K_x = -\frac{\gamma\,\lambda h v_x}{\pi[\gamma^2(x-v_x t)^2+h^2]} \tag{5}$$

where $\gamma = 1/(1-v_x^2/c^2)^{1/2}$. We have also obtained (5) by solving Maxwell's equations in the region above the perfectly conducting plate, where the current density $\boldsymbol{J} = \mathbf{x}\lambda v_x \delta(x-v_x t)\delta(z-h)$ is due to the x-motion of the line charge. Here, δ is the Dirac delta function. Equation (5) reduces to (4) in the nonrelativistic limit, $c \to \infty$. Fig. 2 plots (5) at $t = 0$, where $\beta = v_x/c$. Also shown (black dashed curve) is the electrostatic (RS) limit, (4). Note that for charge motion parallel to flat conducting plates, RS gives a zero total induced current leaving the plates at $x \to \pm\infty$, as also shown in Fig. 2.

For perpendicular motion with a constant velocity, $\mathbf{z}v_z$, we take the electric current density to be

$$\boldsymbol{J} \equiv zJ_z = z\begin{cases} 0, & t<0 \\ \lambda v_z \delta(x)\delta(z-h-v_z t), & t \geq 0. \end{cases} \tag{6}$$

For the single-plate geometry [Fig. 1(a)] in the quasi-static limit, the induced current on the conducting plate is

$$K_x = -\frac{\lambda v_z x}{\pi[x^2+(h+v_z t)^2]} \tag{7}$$

which satisfies the continuity equation (2) after setting $x_c = 0$ and $z_c = h + v_z t$ in (1). We shall show below that the relativistically correct form is given by, [cf., (13) in the single plate limit, $d \to \infty$]

$$K_x = -\frac{\lambda\gamma^2 v_z x}{\pi[x^2+\gamma^2(h+v_z t)^2]} \times \frac{ct + hv_z/c}{\left[(ct)^2 - x^2 - h^2\right]^{1/2}} \tag{8}$$

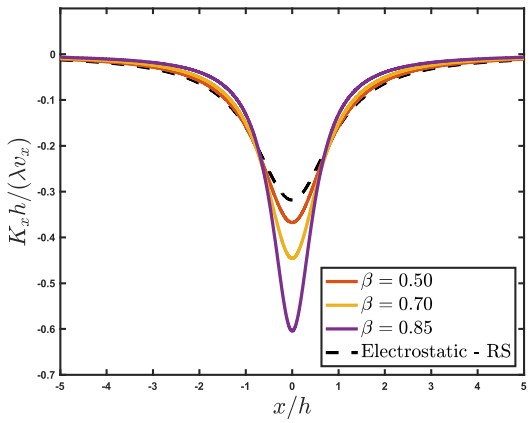

Fig. 2. Induced current in the single-plate geometry [Fig. 1(a)] due to a line charge moving parallel to the conducting plate with $t = 0$, from (5). The "Electrostatic-RS" result is from (4).

where $\gamma = 1/(1-v_z^2/c^2)^{1/2}$. Equation (8) requires that

$$ct > \sqrt{x^2+h^2} \tag{9}$$

which gives the minimum time for the radiation produced by the initial acceleration of the line charge located at $(x, z) = (0, h)$ at $t = 0$ [cf., (6)] to reach the position $(x, 0)$ on the conducting plate. It is clear that (8) reduces to (7) in the nonrelativistic limit, $c \to \infty$. Fig. 3 shows the evolution of $K_x(x;t)$ according to (8). Due to the nature of the Dirac delta functions in $\boldsymbol{J}$, the initial movement of the line charge at $t = 0$ implies that an electromagnetic wave of infinite amplitude is generated at $t = 0$ at $(0, h)$, which reaches the observation position $(x, 0)$ when ct is equal to the right-hand side (RHS) of (9). The singularity in K_x at this instant is apparent in (8) and in Fig. 3. The induced current K_x is zero if the inequality sign in (9) is reversed.

III. Two Parallel Plates

We now consider the perpendicular motion of a line charge inside a parallel-plate geometry [Fig. 1(b)], with the current density given by (6). We shall first consider the induced current for $0 < t < T, T = (d-h)/v_z$, (i.e., before the line charge hits the upper plate at time T). In the quasi-static (RS) regime, we calculate the induced current from an infinite number of image charges, each of which will contribute to a term similar to (7). The infinite sum may be written in closed form, yielding the total induced current on the lower plate, (see Appendix B)

$$K_x = -\frac{\lambda v_z}{2d}\frac{\sinh\left(\frac{x\pi}{d}\right)}{\cosh\left(\frac{x\pi}{d}\right) - \cos\left(\frac{\pi}{d}(v_z t + h)\right)}. \tag{10}$$

Equation (10) gives $K_x \to \mp\lambda v_z/(2d)$ as $x \to \pm\infty$, meaning that a total induced surface current density, $-\lambda v_z/d$, leaves the lower conducting plate at large $|x|$, a well-known result of RS [1], [2] for this geometry. The detailed induced current distribution is shown by the black dashed lines in Figs. 4 and 5. It is straightforward to verify that (10) reduces to (7) in the single-plate limit, $d \to \infty$.

The exact solution for the surface current on the lower plate [Fig. 1(b)], from Maxwell's equations using (6) as a source,

This article has been accepted for inclusion in a future issue of this journal. Content is final as presented, with the exception of pagination.

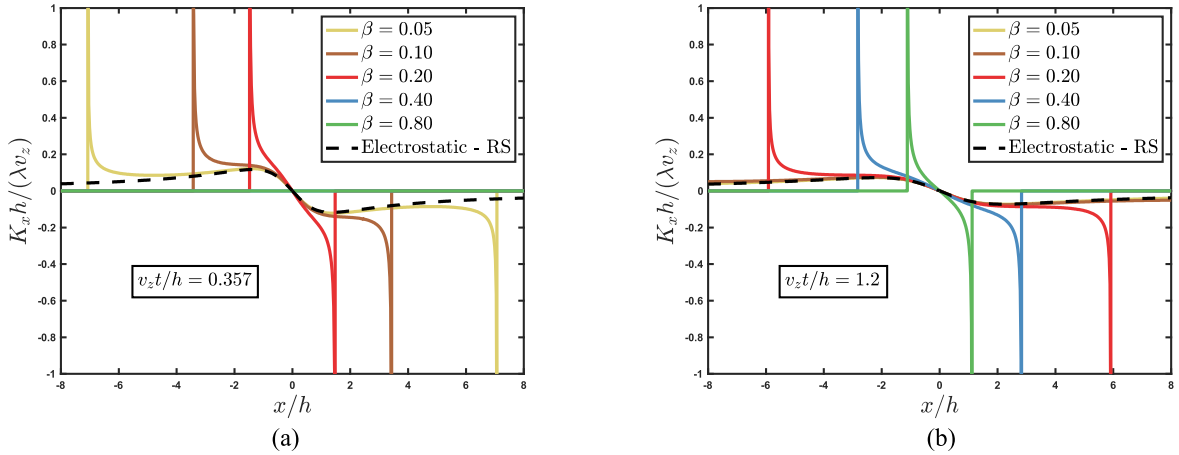

Fig. 3. Induced current computed from (8), for a line charge moving perpendicular to a single conducting plate shown in Fig. 1(a), evaluated at (a) $v_z t/h = 0.357$, and (b) $v_z t/h = 1.2$. The electrostatic limit, corresponding to the RS results, (7), is shown by the black dashed line.

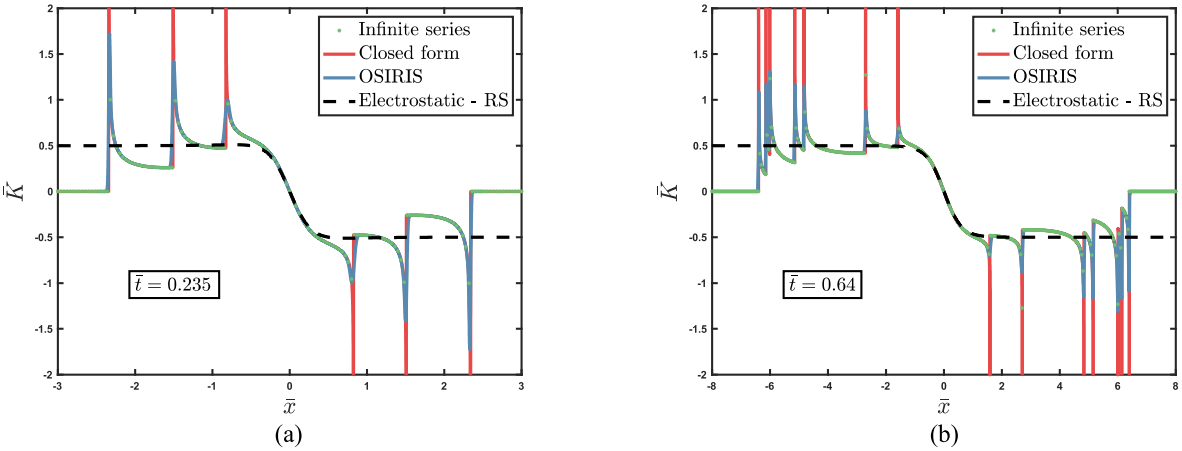

Fig. 4. Validation of the electromagnetic induced current distribution for a line charge moving perpendicular to two parallel plates [Fig. 1(b)] with $\beta = 0.1$, $\bar{h} = 0.2$ and (a) $\bar{t} = 0.235$ and (b) $\bar{t} = 0.64$, using three very different numerical algorithms: Infinite series [see (11), in green], closed-form solution [see (13), or (14a), in red], and OSIRIS code [in blue]. Also included are the quasi-static results [see (10), black dashed line] for comparison. Note that in this figure, the line charge has not hit the upper plate, which occurs at $\bar{t} = \bar{T} = 0.8$.

may be written, (see Appendix C)

$$\begin{aligned}\bar{K}_x(x;t) &= -\frac{1}{2\pi i}\int_\Gamma d\bar{s}e^{\bar{s}\bar{t}}\left\{e^{-\bar{s}\beta\bar{x}}\frac{1}{2\bar{s}}\left(1-e^{-\bar{s}(1-\bar{h})}\right)\right.\\ &\quad+\sum_{n=1}^{\infty}e^{-\left(\bar{s}^2\beta^2+n^2\pi^2\right)^{1/2}\bar{x}}\frac{n\pi}{\bar{s}^2+n^2\pi^2}\\ &\quad\left.\times\left[-\sin\left(n\pi\bar{h}\right)+\frac{\bar{s}}{n\pi}\left(\cos\left(n\pi\bar{h}\right)-(-1)^n e^{-\bar{s}(1-\bar{h})}\right)\right]\right\}\end{aligned} \tag{11}$$

where $\bar{K}_x(x;t) = K_x/(\lambda v_z/d)$, $\bar{s} = sd/v_z$, $\beta = v_z/c$, $\bar{h} = h/d$, $\bar{t} = v_z t/d$, and $\bar{x} = x/d$, and where Γ is the Bromwich contour for the inversion of the Laplace transform in t. The integral contains contributions from the poles at $\bar{s} = in\pi$ and from the branch cuts originating at $\bar{s} = in\pi/\beta, n = 0, \pm1, \pm2, \ldots,$. Appendix C shows that the contributions from the poles add up to

$$\bar{K}_x^{(\text{poles})}(x;t) = -\frac{1}{2}\frac{\sinh\left(\frac{\pi\bar{x}}{\gamma}\right)}{\cosh\left(\frac{\pi\bar{x}}{\gamma}\right)-\cos(\pi(\bar{t}+\bar{h}))} \tag{12}$$

where $\gamma = 1/(1-v_z^2/c^2)^{1/2}$. This partial solution reduces to (10) in the nonrelativistic limit, $\gamma = 1$. Equation (12) may also be obtained from a similar image charge method with Lorentz transform that leads to (5) (now with an infinite number of image line charges for two parallel plates [Fig. 1(b)]). It is also contained in the exact expression for the induced current on the lower plate [Fig. 1(b)], which is plotted in Figs. 4 and 5.

Fig. 4 includes comparisons with simulation results using a 2-D particle-in-cell code, Object-oriented Simulation Rapid Implementation System (OSIRIS) [11], [12]. These simulations used an electron beam with Gaussian density profiles in the x- and z-directions with a standard deviation of 0.25 c/ω_p in each direction, where the plasma frequency ω_p corresponds to an electron density $n_0 = 2.7 \times 10^{25}$ m^{-3}.

This article has been accepted for inclusion in a future issue of this journal. Content is final as presented, with the exception of pagination.

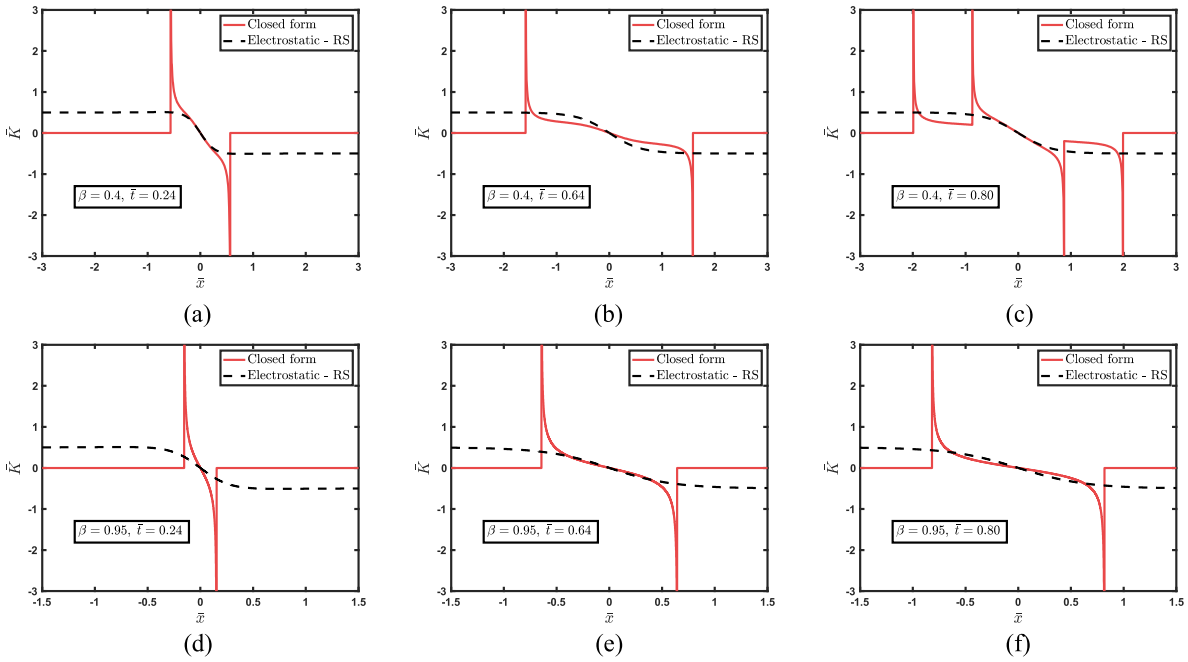

Fig. 5. Comparison of the closed-form electromagnetic and electrostatic induced current distribution for a line charge moving perpendicular to two parallel plates [Fig. 1(b)] with $\bar{h} = 0.2$. (a)–(c) Top row, a mildly relativistic velocity, $\beta = 0.4$. (d)–(f) Bottom row, a relativistic velocity, $\beta = 0.95$. In each row, the surface current distribution on the lower conducting plate is shown at $\bar{t} = 0.24, 0.64,$ and 0.80^{-}, from left to right [$\bar{t} = 0.80^{-}$ denotes the time shortly before the line charge hits the upper plate].

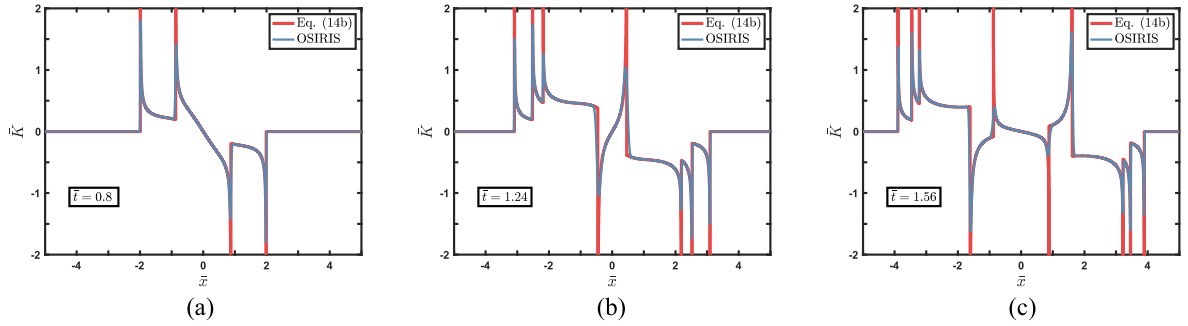

Fig. 6. Comparison between the closed-form electromagnetic solution [see (14b)] and OSIRIS code of the induced current distribution after the vertically-moving line charge hits the upper plate [Fig. 1(b)] with $\bar{h} = 0.2$, $\beta = 0.4$ and (a) $\bar{t} = 0.8$, (b) $\bar{t} = 1.24$, and (c) $\bar{t} = 1.56$. The line charge hits the upper plate at $\bar{t} = \bar{T} = 0.8$, after which it is removed. Note that the red curves are identical in Part (a) and in Fig. 5(c), computed at $\bar{t} = 0.80^{+}$ and $\bar{t} = 0.80^{-}$, respectively. The electrostatic induced current distribution (not shown) is identically equal to zero because $\bar{t} > \bar{T}$.

The beam was specified to travel at a constant velocity in the $+z$-direction, toward the upper plate. The simulation region of linear dimensions $(480 \times 30)\ c/\omega_p$ was set up with the upper and lower walls set as "conducting" boundaries. The simulation results are displayed in Fig. 4, which shows remarkable agreement with the numerical evaluation of (11), and with the analytic solution, (13), given below.

We show in Appendix D that (11) may be reduced to the closed form

$$\bar{K}_x(x;t) = -\sum_n{}' \left\{ \frac{\bar{x}\left[\bar{t}/\beta + \left(\bar{h} - 2n\right)\beta\right]}{\pi\left[\left(\bar{t}/\beta\right)^2 - \bar{x}^2 - \left(\bar{h} - 2n\right)^2\right]^{1/2}\left[\left(\bar{t} + \bar{h} - 2n\right)^2 + \bar{x}^2/\gamma^2\right]} \right\} \equiv \boldsymbol{K}(\bar{x}, \bar{t}, \bar{h}) \tag{13}$$

where the sum $\sum_n{}'$ is over those integer values of n (positive, zero, and negative) such that the argument of the square root in the summand is positive. In the single-plate limit, $d \to \infty$, only the $n = 0$ term remains in (13), which becomes (8) given above. The induced current is infinite when the square root in the denominator of (13) vanishes. This occurs at the time it takes light to reach a position x on the bottom plate, from the initial location of an arbitrary image line charge. Alternatively, at a given t, the field infinity occurs at a position x (see Fig. 4) on the lower plate where light just arrives from the initial location of an image line charge.

Fig. 5 shows the electromagnetic induced current distribution calculated using (13) for mildly relativistic and relativistic velocities v_z, up to the time the line charge is about to hit the top plate at $t = T$, or $\bar{t} = \bar{T} = 1 - \bar{h} = 0.8$ in dimensionless form. The electrostatic results, (10), are included

This article has been accepted for inclusion in a future issue of this journal. Content is final as presented, with the exception of pagination.

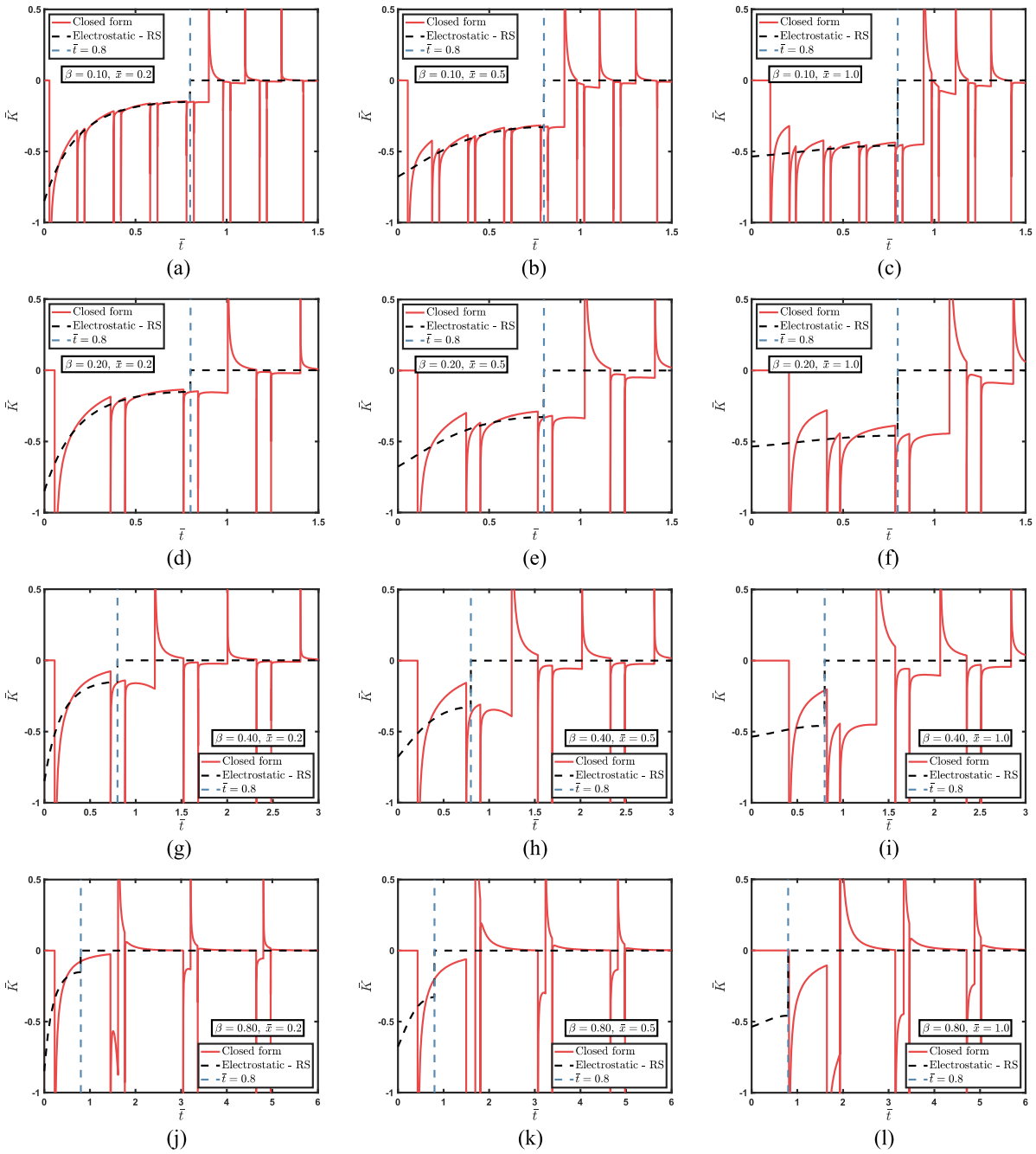

Fig. 7. Comparison of the closed-form electromagnetic and electrostatic induced current distribution with $\bar{h} = 0.2$ and (a)–(c) $\beta = 0.1$, (d)–(f) $\beta = 0.2$, (g)–(i) $\beta = 0.4$, and (j)–(l) $\beta = 0.8$. In each row, the surface current time-evolution on the lower conducting plate is shown at $\bar{x} = 0.2, 0.5$, and 1.0 from left to right. Included in each plot is a vertical line denoting $\bar{t} = \bar{T} = 0.8$, the time at which the line charge strikes the upper plate, and is removed thereafter. The closed-form electromagnetic solution is given by (14a,b). The electrostatic solution is given by (10) for $\bar{t} < \bar{T}$, and is identically equal to zero for $\bar{t} > \bar{T}$.

for comparison. Figs. 4 and 5 show that the electrostatic solution fails to account for electromagnetic transients and multiple reflections, but works rather well otherwise, even for a highly relativistic beam, except near the wavefront(s) where the transient solution dominates. If the line charge is removed after it hits the upper plate at $\bar{t} = \bar{T}$, there is no induced current in the electrostatic RS theory after $\bar{T}$. However, reflection of the electromagnetic waves that exist at $\bar{t} = \bar{T}$ within the plates continues in the electromagnetic theory. In the electromagnetic theory, the induced current on the lower plate is given by (see Appendix E)

$$\bar{K}_x(x;t) = \begin{cases} \boldsymbol{K}\left(\bar{x},\bar{t},\bar{h}\right), & 0 < \bar{t} < \bar{T} \quad (14a) \\ \boldsymbol{K}\left(\bar{x},\bar{t},\bar{h}\right) - \boldsymbol{K}\left(\bar{x},\bar{t}-\bar{T},1\right), & \bar{t} \geq \bar{T} \quad (14b) \end{cases}$$

where $\boldsymbol{K}\left(\bar{x},\bar{t},\bar{h}\right)$ is defined in (13). Fig. 6 shows remarkable agreement between (14b) and OSIRIS simulation results after $\bar{T}$. In Fig. 6, an electromagnetic shock is generated at the upper plate on impact by the upward-moving line charge; this shock causes the spikes in the induced current on the lower

This article has been accepted for inclusion in a future issue of this journal. Content is final as presented, with the exception of pagination.

plate at $\bar{x} = \pm 0.45826$ in Fig. 6(b), and at $\bar{x} = \pm 1.6155$ in Fig. 6(c).

Having shown the almost perfect agreement between OSIRIS with (14a) for $\bar{t} < \bar{T}$ in Fig. 4, and with (14b) for $\bar{t} \geq \bar{T}$ in Fig. 6, we plot in Fig. 7 the temporal evolution of the induced current at various points on the lower plate for all time, and compare this exact electromagnetic solution with the electrostatic solution.

If the line charge moves downward, its coordinates $z = z_0(t) = h - v_z t, (t > 0, v_z > 0)$ will reach the lower plate at time $T = h/v_z$, or $\bar{T} = \bar{h}$ [Fig. 1(b)]. If the line charge is removed after $\bar{T}$, the induced current on the lower plate is found to be also given by (14a,b), in which $\boldsymbol{K}(\bar{x}, \bar{t}, \bar{h})$ is replaced by $\boldsymbol{K}(\bar{x}, -\bar{t}, \bar{h})$, and $\boldsymbol{K}(\bar{x}, \bar{t} - \bar{T}, 1)$ is replaced by $\boldsymbol{K}(\bar{x}, -(\bar{t} - \bar{T}), 0)$. We have once more verified that this analytic solution is in excellent agreement with OSIRIS, both before and after $\bar{T} = \bar{h}$, similar to Figs. 4 and 6. Again, an electromagnetic shock is initiated on the lower plate at time $\bar{T} = \bar{h}$, when the downward-moving line charge hits the lower plate and is removed afterward.

IV. Conclusion

The RS theorem is a foundational result in electronics, used widely in modern computational models of vacuum electronics, discharge physics, and semiconductor devices. The original theorem was derived by assuming quasi-static fields, ignoring both relativistic and radiative effects. The article presents simple, solvable examples in which this assumption is relaxed, and examines the magnitude of the corrections. While it is clear that the electrostatic solution fails to account for electromagnetic transients and multiple reflections, Figs. 4 and 5 show that it works rather well otherwise, even for a highly relativistic beam, except near the wavefront(s) where the transients dominate. This perhaps partially explains the mystery as to why the nonrelativistic RS has been very successful in the description of traveling wave tubes and klystrons [4], where only the sinusoidal steady solutions are considered, that is, ignoring transients but fully accounting for all reflections in the electromagnetic eigenmode solutions, even if the electron beam is highly relativistic. However, the complexity in the reflected waves, as shown in Figs. 4 and 7 even for the most basic parallel plate geometry, seems to have resisted progress on an electromagnetically and relativistically correct version of the general RS theorem for more than 80 years.

Our exact closed-form solutions have been confirmed by several methods, so they can be confidently used in practical applications. For example, in modern satellite communication, multipactor discharge is a major concern [13]. The parallel plates may represent a planar transmission line, and the line charge may represent an electron generated by multipactor discharge [7], [14]. The induced current on the wall that we calculated here provides a direct measure of the degree of contamination on the quality of a signal (analog or digital) that is carried on the transmission line. Indeed, such considerations partly motivated this study, beyond the classical RS. Here, we find that the induced current in the form of an electromagnetic shock is generated when a "multipactoring" electron strikes a surface, a feature absent in RS and in all existing analyses of multipactor. The extent to which this purely electromagnetic phenomenon affects signal quality remains to be quantified [14].

Finally, we have tried to repeat our calculations of the induced current for the case of a point charge. The problem becomes 3-D, far more complicated than the 2-D problem of a line charge studied in this article. Our preliminary study shows that the induced current due to a point charge behaves qualitatively the same as a line charge.

Appendix A. Derivation of (5)

We use the image charge method. In the rest frame of the line charge moving with velocity $\mathbf{v} = \mathbf{x} v_x$ relative to the lab frame, there is an electric field $\mathbf{E} = \mathbf{z} E_z = \mathbf{z}\sigma/\epsilon_0$ at the surface of the conducting plate, where σ is given by (1). The Lorentz transformation back to the lab frame is given by

$$\mathbf{E}'_\perp = \gamma\,(\mathbf{E}_\perp + \mathbf{v} \times \mathbf{B}) \tag{A.1}$$

$$\mathbf{B}'_\perp = \gamma \left(\mathbf{B}_\perp - \frac{1}{c^2}\mathbf{v} \times \mathbf{E}\right) \tag{A.2}$$

$$\mathbf{x}'_\perp = \mathbf{x}_\perp, \mathbf{x}'_\parallel = \gamma\,(\mathbf{x}_\parallel - \mathbf{v}t) \tag{A.3a, b}$$

$$\gamma = 1/(1 - v^2/c^2)^{1/2} \tag{A.4}$$

where [unprimed, primed] quantities are measured in the [moving, lab] frame. Equation (A.2) gives

$$\mathbf{H}'_\perp = -\gamma\,\epsilon_0 \mathbf{v} \times \mathbf{E} \tag{A.5}$$

since $\mathbf{B} = 0$ in the moving frame. This yields

$$H'_y = \frac{\gamma\, v_x \lambda h}{\pi\,[\gamma^2 (x - v_x t)^2 + h^2]} \tag{A.6}$$

from which it follows that the surface current $\mathbf{K}' = \mathbf{z} \times \mathbf{H}'$ on the conducting plate in the lab frame is given by (5) in the text.

Appendix B. Derivation of (10)

A static line charge located at $(x, z) = (0, z_c)$ between two parallel plates separated by distance d [Fig. 1(b)] induces an infinite number of image line charges located at $(0, z_c + 2\text{nd})$ and $(0, -z_c + 2\text{nd})$, $n = 0, \pm 1, \pm 2, \pm 3, \ldots,$. The line charge and its images induce a surface charge on the lower plate given by

$$\sigma = -\frac{\lambda}{2\pi} \sum_{n=-\infty}^{\infty} \left[\frac{(h + v_z t) + 2nd}{x^2 + ((h + v_z t) + 2nd)^2} - \frac{-(h + v_z t) + 2nd}{x^2 + (-(h + v_z t) + 2nd)^2} \right]. \tag{B.1}$$

Each term within this infinite sum may be compared with (1). Consequently, analogous to (7), we obtain the induced current on the lower plate as a sum over image charges

$$K_x = -\frac{\lambda v_z x}{2\pi} \sum_{n=-\infty}^{\infty} \left[\frac{1}{x^2 + ((h + v_z t) + 2nd)^2} - \frac{-1}{x^2 + (-(h + v_z t) + 2nd)^2} \right]. \tag{B.2}$$

This article has been accepted for inclusion in a future issue of this journal. Content is final as presented, with the exception of pagination.

Note that (1) and (7) are the $n = 0$ terms of (B.1) and (B.2), respectively. Using the identity

$$\sum_{n=-\infty}^{\infty} \frac{1}{a^2 + (n+b)^2} = \frac{\pi}{a} \frac{\sinh(2\pi a)}{\cosh(2\pi a) - \cos(2\pi b)} \tag{B.3}$$

we obtain (10) in the text.

Appendix C. Derivation of (11)

For a line charge moving in the z-direction [cf., (6)], the only nonzero component of the magnetic field is H_y, and the only nonzero components of the electric field are E_x and E_z. The z-component of the Maxwell equation involving $\mathbf{J}$ [see (6)] reads

$$\frac{\partial H_y}{\partial x} = J_z + \epsilon_0 \frac{\partial E_z}{\partial t}. \tag{C.1}$$

Away from the line charge, the Helmholtz (wave) equation

$$\nabla^2 \tilde{H}_y(z, x; s) - \frac{s^2}{c^2} \tilde{H}_y(z, x; s) = 0 \tag{C.2}$$

is written in terms of the Laplace transform of H_y, defined as

$$H_y(z, x; t) = \frac{1}{2\pi i} \int_{\Gamma} ds e^{\mathrm{st}} \tilde{H}_y(z, x; s) \tag{C.3}$$

where Γ is the Bromwich contour. In writing (C.2), we ignore the contributions from the initial values of $\mathbf{E}$ that always accompany the Laplace transform technique (which applies only to $t > 0$), as a detailed examination shows that this initial $\mathbf{E}$ does not contribute to the induced current on the perfect conductor (whereas the initial impulse acceleration of the line charge, implied by (6), would produce the important electromagnetic transients that are absent in the quasistatic approach of Ramo and Shockley). We next express $\tilde{H}_y$ in a Fourier series

$$\tilde{H}_y(z, x; s) = \sum_{n=0}^{\infty} A_n(s) \cos\left(\frac{n\pi z}{d}\right) e^{-K_n x}, \quad x > 0 \tag{C.4a}$$

$$\tilde{H}_y(z, x; s) = \sum_{n=0}^{\infty} B_n(s) \cos\left(\frac{n\pi z}{d}\right) e^{K_n x}, \quad x < 0 \tag{C.4b}$$

$$K_n = \left(\left(\frac{n\pi}{d}\right)^2 + \frac{s^2}{c^2}\right)^{1/2} \tag{C.5}$$

where $\mathrm{Re}(K_n) > 0$. Note that (C.4a) and (C.4b) satisfy the boundary condition on both conducting plates, $(\partial \tilde{H}_y/\partial z) = s\epsilon_0 E_x = 0$ when $z = 0$ and $z = d$. The coefficients, A_n and B_n, are determined from the two conditions at $x = 0$: $\tilde{E}_z$ is continuous and $\tilde{H}_y$ suffers a finite jump according to (C.1) and (6). The induced current density on the lower conducting plate then equals $-H_y(0, x; t)$, which may be written in dimensionless variables as (11), for $x > 0$.

The Bromwich contour Γ in (11) may be deformed to include the contributions from the simple poles, located at $\bar{s} = in\pi$, and the contributions from the path integrals on both sides of the branch cuts, each of which originates from a branch point, located at $\bar{s} = in\pi/\beta, n = 0, \pm 1, \pm 2, \ldots,$. It is straightforward to show that the contributions from the simple poles yield

$$\bar{K}_x^{(\mathrm{poles})}(x; t) = -\frac{1}{2} - \sum_{n=1}^{\infty} \cos\left[n\pi\left(\bar{t} + \bar{h}\right)\right] e^{-n\pi \bar{x}/\gamma} \tag{C.6}$$

which may be shown to be the same as (12). The branch cut contributions may be written as,

$$\begin{aligned} &\bar{K}_x^{(bc)}(x; t) \\ &= \frac{2}{\pi} \sum_{n=1}^{\infty} \int_1^{\infty} \frac{d\xi}{\xi^2 - \beta^2} \sin\left[\left(\xi^2 - 1\right)^{1/2} n\pi \bar{x}\right] \\ &\quad \times \left[\xi \cos\left(\frac{\xi}{\beta} n\pi \bar{t}\right) \cos\left(n\pi \bar{h}\right) - \beta \sin\left(\frac{\xi}{\beta} n\pi \bar{t}\right) \sin(n\pi \bar{h})\right]. \end{aligned} \tag{C.7}$$

We note that (C.7) exhibits highly oscillatory behavior, making any numerical evaluation with more than four significant figures difficult to obtain. In Fig. 4, we also numerically confirm that (C.7) is divergent when $\bar{t} = \beta[\bar{x}^2 + (\bar{h} - 2n)^2]^{1/2}$, $n = 0, \pm 1, \pm 2, \ldots,$ as predicted by the exact, closed-form solution, (13). The numerical solution to (11), including the divergence of the solutions, agrees extremely well with the closed-form expression, (13), and with the 2-D OSIRIS PIC simulation, as illustrated in Fig. 4.

Appendix D. Derivation of (13)

In this appendix, we derive the closed-form induced current solution on the lower plate, (13). Here, we use the Fourier representations, for $-\infty < x < \infty$

$$\tilde{g}(k) = \int_{-\infty}^{\infty} dx e^{ikx} g(x) \tag{D.1a}$$

$$g(x) = \frac{1}{2\pi} \int_{-\infty}^{\infty} dk e^{-ikx} \tilde{g}(k). \tag{D.1b}$$

To satisfy the boundary condition $(\partial \tilde{H}_y/\partial z) = s\epsilon_0 E_x = 0$ when $z = 0$ and $z = d$, we express $\tilde{E}_x$, $\tilde{E}_z$, and $\tilde{H}_y$ as Fourier series

$$\tilde{E}_x = \sum_{m=0}^{\infty} \tilde{E}_{xm} \sin(\kappa_m z) \tag{D.2a}$$

$$\tilde{E}_z = \sum_{m=0}^{\infty} \tilde{E}_{zm} \cos(\kappa_m z) \tag{D.2b}$$

$$\tilde{H}_y = \sum_{m=0}^{\infty} \tilde{H}_{ym} \cos(\kappa_m z) \tag{D.3}$$

where $\kappa_m = (m\pi/d), m = 0, 1, 2, \ldots,$. Define $\omega_m = c(\kappa_m^2 + k^2)^{1/2}$ and write the current density

$$\boldsymbol{J} \equiv \boldsymbol{z} J_z = \boldsymbol{z} \begin{cases} 0, & t < 0 \\ \lambda \dot{z}_0(t) \delta(x) \delta(z - z_0(t)), & T > t \geq 0 \end{cases} \tag{D.4}$$

in terms of the z-location of the line charge, $z_0(t)$. T is the time of flight from $z = h$ to $z = d$. The time evolution of

This article has been accepted for inclusion in a future issue of this journal. Content is final as presented, with the exception of pagination.

$\tilde{H}_{ym}$ is governed by

$$\frac{\partial^2 \tilde{H}_{ym}}{\partial t^2} + \omega_m^2 \tilde{H}_{ym} = ikc^2 \epsilon_m K(t) \cos(\kappa_m z_0(t)) \quad \text{(D.5)}$$

$$\epsilon_m = \begin{cases} 1, & m = 0 \\ 2, & m > 0 \end{cases} \quad \text{(D.6)}$$

where $K(t) \equiv \lambda \dot{z}_0(t)/d$. We apply the initial conditions $\tilde{H}_{ym}(t=0) = 0$ [assuming that $\dot{z}_0(t=0) = 0$] and $(\partial \tilde{H}_{ym}/\partial t)(t=0) = 0$ [assuming that the initial electric field is electrostatic] and solve (D.5) for $\tilde{H}_{ym}(t)$. We then compute the inverse Fourier transform and find, using [15, eq. (ET I 26(30))]

$$H_{ym} = \begin{cases} 0, & t \le \dfrac{|x|}{c} \\ -\dfrac{c}{2}\epsilon_m \displaystyle\int_0^{t-\frac{|x|}{c}} dt' K(t') \cos\big(\kappa_m z_0(t')\big) & \\ \times \dfrac{\partial}{\partial x} J_0\Big[\kappa_m \Big(c^2(t-t')^2 - x^2\Big)^{1/2}\Big], & t > \dfrac{|x|}{c} \end{cases} \quad \text{(D.7)}$$

where J_0 is the Bessel function of the first kind of order zero. Summing over m, we find from (D.3) and (D.1b), applying [15, eqs. (MO 59) and (MO 60)]

$$H_y(x,z;t) = -\frac{c}{2}\int_0^{t-\frac{|x|}{c}} dt' K(t') \times \frac{\partial}{\partial x}\big[S(a,b^+) + S(a,b^-)\big], \quad T > t > \frac{|x|}{c} \quad \text{(D.8)}$$

where $a \equiv (\pi/d)(c^2(t-t')^2 - x^2)^{1/2}$, $b = b^{\pm} \equiv |z \pm z_0|/(c^2(t-t')^2 - x^2)^{1/2}$ and

$$S(a,b) = \frac{1}{2} + \sum_{m=1}^{\infty} J_0(ma)\cos(mab) = \begin{cases} \dfrac{1}{a(1-b^2)^{1/2}} + \displaystyle\sum_{l=1}^{M_1} \frac{1}{\big(a^2 - (2\pi l + ab)^2\big)^{1/2}} & \\ \quad + \displaystyle\sum_{l=1}^{N} \frac{1}{\big(a^2 - (2\pi l - ab)^2\big)^{1/2}}, & b < 1 \\ \displaystyle\sum_{l=M_2+1}^{N} \frac{1}{\big(a^2 - (2\pi l - ab)^2\big)^{1/2}}, & b \ge 1. \end{cases} \quad \text{(D.9)}$$

In (D.9), $M_{1,2}$ and N are defined by

$$2\pi M_1 < a(1-b) < 2\pi(M_1+1) \quad \text{(D.10a)}$$

$$2\pi M_2 < a(b-1) < 2\pi(M_2+1) \quad \text{(D.10b)}$$

$$2\pi N < a(1+b) < 2\pi(N+1). \quad \text{(D.10c)}$$

Equation (D.8) may be written as

$$H_y(x,z;t) = -c\frac{\lambda v_z}{d}\left[\int dt' \frac{\partial}{\partial x}\left\{\sum_l{}'\left[\frac{1}{\big(a^2 - (2\pi l - ab)^2\big)^{1/2}}\right]\right\}\right]_{t'=0}^{t'=t-\frac{|x|}{c}} = c\frac{\lambda v_z}{d}\left[\int dt' \frac{\partial}{\partial x}\left\{\sum_l{}'\left[\frac{1}{\big(a^2 - (2\pi l - ab)^2\big)^{1/2}}\right]\right\}\right]_{t'=0} \quad \text{(D.11)}$$

where the sum $\sum_l'$ is over those integer values of l such that the argument of the square root in the summand is positive. In writing the last equality in (D.11), we note that the integral is 0 at $t' = t - |x|/c$. We remark that (D.11) is valid only for $t < T$. Setting $z = 0$ and assuming impulse acceleration at $t = 0$, i.e., $z_0(t) = h + v_z t$, $(t > 0)$, we obtain from (D.11)

$$H_y(x,0;t) = \frac{1}{c}\frac{\lambda v_z}{d} \times \sum_n{}'\left\{\frac{xd[c^2t + (h+2nd)v_z]}{\pi\big[(ct)^2 - x^2 - (h-2nd)^2\big]^{1/2}\big[(v_z t + h - 2nd)^2 + x^2/\gamma^2\big]}\right\} \quad \text{(D.12)}$$

which is (13), upon converting to dimensionless variables.

Appendix E. Derivation of (14)

If the line charge is removed after it hits the upper plate at time $t = T = (d-h)/v_z$, the current density in this parallel plate geometry [Fig. 1(b)] is rewritten to emphasize its absence for $t > T$

$$\boldsymbol{J} \equiv z J_z(t)[H(t) - H(t-T)] \quad \text{(E.1)}$$

where $J_z(t) = \lambda v_z \delta(x)\delta(z - h - v_z t)$ is the same as in (6) and $H(t)$ is the Heaviside unit step function. For $t < T$, only the first term in (E.1) would contribute to the induced current which is given by (13), thus (14a).

Note that the solution (13) continues for $t > T$, without any change in its behavior, as if $J_z(t)$ continues to persist from $t = T$ to $t = \infty$. Thus, for $t > T$, we need to subtract from the solution (13) the contribution that is due to the second term in (E.1). The result is (14b), which we prove next.

To evaluate the contribution due only to the second term in (E.1), for $t > T$, the technique in Appendix D leads to a similar initial value problem, in which (D.5) becomes

$$\frac{\partial^2 \tilde{H}_{ym}}{\partial t^2} + \omega_m^2 \tilde{H}_{ym} = -ikc^2 \epsilon_m (\lambda v_z/d)\cos(\kappa_m(h + v_z t)), \quad t > T \quad \text{(E.2)}$$

$$\tilde{H}_{ym}(t=T) = 0 \quad \text{(E.3)}$$

$$\frac{\partial \tilde{H}_{ym}}{\partial t}(t=T) = 0. \quad \text{(E.4)}$$

The minus sign in the RHS of (E.2) accounts for the minus sign in the second term of (E.1), and the initial conditions (E.3) and (E.4) mean that we are just removing the current source for $t > T$, leaving the electromagnetic fields caused by

This article has been accepted for inclusion in a future issue of this journal. Content is final as presented, with the exception of pagination.

the first term of (E.1) unchanged at $t = T$. Letting $t' = t - T$, (E.2)–(E.4) become

$$\frac{\partial^2 \tilde{H}_{ym}}{\partial t'^2} + \omega_m^2 \tilde{H}_{ym} = -ikc^2 \epsilon_m (\lambda v_z/d) \cos\left(\kappa_m \left(d + v_z t'\right)\right), \quad t' > 0 \tag{E.5}$$

$$\tilde{H}_{ym}\left(t' = 0\right) = 0 \tag{E.6}$$

$$\frac{\partial \tilde{H}_{ym}}{\partial t'}\left(t' = 0\right) = 0. \tag{E.7}$$

Equations (E.5)–(E.7) are exactly of the same form as (D.5) and its associated zero initial conditions that follow. The same procedure then led to the solution (D.12) in which t is replaced by $t' = t - T$ and h is replaced by d. We thus obtain (14b) in nondimensional form. Fig. 6 shows that (14b) is in excellent agreement with OSIRIS for $t \geq T$.

ACKNOWLEDGMENT

The authors would like to acknowledge useful discussions with Prof. Alec Thomas and Prof. Zhong He of the University of Michigan, and Prof. Warren Mori of the University of California, Los Angeles (UCLA). They would also like to thank the OSIRIS Consortium, consisting of UCLA and Instituto Superior Tecnico (IST) (Lisbon, Portugal) for providing access to the OSIRIS 4.0 framework.

REFERENCES

[1] S. Ramo, "Currents induced by electron motion," *Proc. IRE*, vol. 27, no. 9, pp. 584–585 Sep. 1939.
[2] W. Shockley, "Currents to conductors induced by a moving point charge," *J. Appl. Phys.*, vol. 9, no. 10, pp. 635–636, Oct. 1938.
[3] G. F. Knoll, *Radiation Detection and Measurement*, 4th ed. Hoboken, NJ, USA: Wiley, 2010.
[4] W. Gewartowski and H. A. Watson, *Principles of Electron Tubes, Including Grid-Controlled Tubes, Microwave Tubes, and Gas Tubes*. New York, NY, USA: Van Nostrand, Jul. 1965.
[5] J. D. Lawson, *The Physics of Charged-Particle Beams*. London, U.K.: Oxford Univ. Press, 1977.
[6] S. Humphries, *Charged Particle Beams*. New York, NY, USA: Wiley, 1990.
[7] R. Kishek, Y. Y. Lau, L. K. Ang, A. Valfells, and R. M. Gilgenbach, "Multipactor discharge on metals and dielectrics: Historical review and recent theories," *Phys. Plasmas*, vol. 5, no. 5, pp. 2120–2126, May 1998.
[8] Z. He, "Review of the Shockley–Ramo theorem and its application in semiconductor gamma-ray detectors," *Nucl. Instrum. Methods Phys. Res. A: Accel. Spectrom. Detect. Assoc. Equip.*, vol. 463, pp. 250–267, May 2001.
[9] B. Pellegrini, "Electric charge motion, induced current, energy balance, and noise," *Phys. Rev. B: Condens. Matter*, vol. 34, pp. 5921–5924, Oct. 1986.
[10] B. Eisenberg and W. Nonner, "Shockley–Ramo theorem measures conformation changes of ion channels and proteins," *J. Comput. Electron.*, vol. 6, nos. 1–3, pp. 363–365, Apr. 2007.
[11] R. A. Fonseca *et al.*, "OSIRIS: A three-dimensional, fully relativistic particle in cell code for modeling plasma based accelerators," in *Proc. Int. Conf. Comput. Sci.*, in Lecture Notes in Computer Science, vol. 2331, Apr. 2002, pp. 342–351.
[12] R. G. Hemker, "Particle-in-cell modeling of plasma-based accelerators in two and three dimensions," 2015, *arXiv:1503.00276*. [Online]. Available: http://arxiv.org/abs/1503.00276
[13] F. Piro and Y. Brand, "PIM and multipactor considerations for future high-RF power space missions," in *Proc. 8th Eur. Conf. Antennas Propag. (EuCAP)*, Apr. 2014, pp. 1643–1646.
[14] P. Y. Wong, Y. Y. Lau, P. Zhang, N. Jordan, R. M. Gilgenbach, and J. Verboncoeur, "The effects of multipactor on the quality of a complex signal propagating in a transmission line," *Phys. Plasmas*, vol. 26, no. 11, Nov. 2019, Art. no. 112114, doi: 10.1063/1.5125408.
[15] I. S. Gradshteyn, I. M. Ryzhik, and D. Zwillinger, *Table of Integrals, Series, and Products*, 8th ed. New York, NY, USA: Academic, 2014.

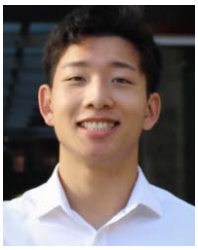

Dion Li (Student Member, IEEE) is currently pursuing the B.S.E. degree in engineering physics with the University of Michigan, Ann Arbor, MI, USA.

His research interests include electromagnetic theory, crossed-field diodes, and plasma wakefield acceleration.

David Chernin received the Ph.D. degree in applied mathematics from Harvard University, Cambridge, MA, USA, in 1976.

He has been with Leidos Inc., Reston, VA, USA, and its predecessor company SAIC, McLean, VA, USA, since 1984, where he has conducted research on beam-wave interactions and other topics in the physics of particle accelerators and vacuum electron devices.

Y. Y. Lau (Fellow, IEEE) received the B.S., M.S., and Ph.D. degrees in electrical engineering from the Massachusetts Institute of Technology, Cambridge, MA, USA, in 1968, 1970, and 1973, respectively.

He is currently a Professor with the University of Michigan, Ann Arbor, MI, USA, where he is specialized in RF sources, heating, and discharge.

Dr. Lau was elected Fellow of the American Physical Society (APS) in 1986, and IEEE Fellow in 2007. He was the recipient of the 1999 IEEE Plasma Science and Applications Award and the 2017 IEEE John R. Pierce Award for Excellence in Vacuum Electronics. He served three terms as an Associate Editor for *Physics of Plasmas* from 1994 to 2002.